LA-UR- 08-7253

Approved for public release;
distribution is unlimited.

Title:	Uncooled infrared and terahertz detectors based on micromechanical mirror as a radiation pressure sensor
Author(s):	Gennady Berman/LANL/T-4/115063 Boris Chernobrod/LANL/T-4/199839 Alan Bishop/LANL/ADTSC/088538 Vyacheslav Gorshkov/LANL/T-4
Intended for:	SFIE Phototomics West

Los Alamos
NATIONAL LABORATORY
EST.1943

Uncooled infrared and terahertz detectors based on micromechanical mirror as a radiation pressure sensor

Gennady P. Berman*[a], Boris M. Chernobrod[a], Alan R. Bishop[b], and Vyacheslav N. Gorshkov[a,c]

[a]Theoretical Division, Los Alamos National Laboratory MS 213, Los Alamos, New Mexico 87545;
[b]Theory, Simulation & Computation Directorate, MS B210, Los Alamos National Laboratory;
Los Alamos, New Mexico 87545
[c]87545, & The Institute of Physics, National Academy of Sciences of Ukraine, Nauki Ave. 46, Kiev-39, 03650, MSP-65, Ukraine

ABSTRACT

We consider mid infrared (5 – 25 μm) and terahertz (100 – 1000 μm), room-temperature detectors based on a microcantilever/micromirror sensor of the radiation pressure. The significant enhancement of sensitivity is due the combination of non-absorption detection and a high quality optical microcavity. Applications for spectrometry and imaging is analyzed. It is shown that the radiation pressure sensor potentially has sensitivity at the level or better than the best conventional uncooled detectors.

Keywords: Terahertz, cantilever, radiation pressure, micromirror

I. INTRODUCTION

Improvement of the sensitivity of detection in the mid infrared (5 – 25 μm) and terahertz region (100 – 1000 μm) is very important for many applications including remote sensing of explosive materials, chemical and biological agents, surveillance, night-vision, and medical imaging. Uncooled thermal detectors are very desirable because cooling systems add cost and cause reliability problems that are incompatible with most applications. Recently, significant progress has been demonstrated for uncooled thermal detectors based on microcantilever arrays[1-4]. Microcantilever systems are potentially more sensitive and have shorter response times than conventional thermoelectric and semiconductor solid state detectors. In conventional thermoelectric imagers the temperature rise in each pixel is measured electrically. The electrical connectivity to each pixel causes prohibitive complexity and cost. A microcantilever-based imager could have full optical readout, eliminating readout electronics, a very attractive feature. Currently microcantilever-based detectors exploit the thermo-mechanical effect, in which a bilayer microcantilever illuminated by radiation exhibits banding due to the difference in the thermal expansion coefficients of the different layers. This measurement method has some limitations related to temperature fluctuations due to heat and radiation exchange with the environment. In the present paper, we propose to utilize the radiation pressure to measure the radiation power. This is less sensitive to temperature fluctuations. We showed recently[5,6] that, using the radiation pressure, the microcantilever detector significantly improves the sensitivity of frequency modulation spectroscopy. One of the significant advantages of radiation pressure measurements is the possibility of using a high quality microcavity, which leads to a significant sensitivity enhancement due to this non-absorption mechanism of detection. Note that application of an optical microcavity to absorption detectors leads to a moderate enhancement of sensitivity because absorption at the photosensitive surface affects the quality of optical resonator. We consider two applications: i) a narrowband heterodyne detector and ii) a broadband detector. The narrowband heterodyne detector could be used as a miniature spectrometer. The broadband detector potentially could be used as a new type of thermal imager. For narrowband detectors, a microcantilever senses the beats between the heterodyne field and the spectral components of the signal. The frequencies of those signal spectral components which we detect are shifted to the red and blue relative to the heterodyne

* gpb@lanal.gov; phone: 505-667 2489; fax 505-665 3003

frequency by an amount equal to the cantilever resonance frequency. The spectrum of the signal can be scanned by tuning the heterodyne frequency. Fortunately, compact, uncooled far infrared solid state lasers are available[7,8]. Application of standard microcavity techniques gives an additional increase in sensitivity due to cavity enhancements of both the heterodyne and the signal fields. In the present paper, we describe the results of our theoretical analysis and numerical simulations of the microcantilever-based detectors schematically depicted in Figs. 1 and 2. We show that i) the proposed narrowband detector is expected to have a sensitivity higher than the typical sensitivity of conventional uncooled far infrared (terahertz) detectors, and ii) the broadband detector potentially has the same sensitivity as the best conventional uncooled thermal detectors with comparable pixel size.

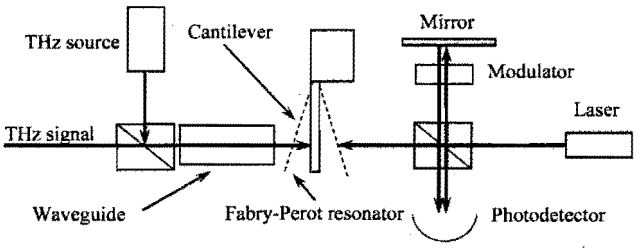

Fig. 1. Setup of the microcantilever based narrowband heterodyne detector.

II. SENSITIVITY ANALYSIS OF A NARROW BAND HETERODINE DETECTOR

Figure 1 shows a possible setup for a microcantilever-based narrowband detector as a radiation pressure sensor. This optical scheme is similar to that used for efficient laser cooling of microcantilevers[9,10], which could cool these microcantilevers to their quantum mechanical ground states. The radiation of the heterodyne laser is mixed with the signal and sent through an optical waveguide, the other end of which is polished and coated with a high reflectivity material (for example a Bragg mirror). The coated waveguide end, in combination with the coated surface of the cantilever, form a Fabry-Perot optical resonator. The cantilever oscillations are measured by a Michelson interferometer. We use a model that describes the oscillations of the cantilever as a damped harmonic oscillator driven by light pressure and thermal noise. The fields in the Fabry-Perot cavity are described by resonator equations, which include damping and incident waves. The electromagnetic fields are written in the form

$$E = \frac{1}{2}\left(E_h(t)\exp(-i\omega_h t) + E_s(t)\exp(-i\omega_s t)\right) + c.c., \tag{1}$$

where $E_{h,s}(t)$, $\omega_{h,s}$ are the amplitude and the frequency of the heterodyne and signal fields, correspondingly. The slow field amplitudes inside the resonator satisfy the following equations:

$$\frac{dE_{h,s}}{dt} = -\frac{1}{\tau_p}\left(E_{h,s} - E^0_{h,s}(t)\right), \tag{2}$$

where the damping time of the resonator is $2\tau_p^{-1} = (1-R)c/(2L\sqrt{R})$, $R = R_1R_2$, $R_{1,2}$ are the reflection coefficients of the fiber end and the microcantilever surface, correspondingly, and L is the average resonator length. In the case of steady-state field amplitudes, $E^0_{h,s}$, are

$$E^0_{h,s} = \frac{E^{ext}_{h,s}T_0}{1-\mathrm{R}\exp(\delta_{h,s})}. \tag{3}$$

In (3) T_0 is the transparency coefficient of the waveguide end, $E^{ext}_{h,s}(t)$ are the external fields launched into the resonator (below, we will consider a more general case when $E^0_{h,s}$ are time-dependent), $\delta_{h,s} = 2k_{h,s}(L+x)$ is the phase of the round-trip pass through the resonator; x is the coordinate of the microcantilever; and $k_{h,s}$ are the wave numbers.

The motion of the microcantilever is described by the equation for a harmonic oscillator perturbed by radiation pressure and thermal noise:

$$\ddot{x} + \Gamma\dot{x} + \omega_0^2 x = A\left|E_h\right|^2 + A\left[E_h^* E_s \exp\left(-i\omega_0 t\right) + c.c.\right] + \frac{F}{m}, \tag{4}$$

where $A = \frac{S}{4\pi m}$, S is the area of microcantilever surface, m is the microcantilever mass; Γ is the damping rate, and F is the thermal noise force. We assume that the difference between the heterodyne frequency and the signal currier frequencyis equal to the cantilever fundamental frequency $\omega_0 = \omega_h - \omega_s$. We assume that the intensity noise of heterodyne laser is negligibly small. In Section III we analyze the influence of the intensity noise and derive the conditions for our assumptions to be correct. Thus, the first term on the right side of Eq. (4) is constant. It is known[9] that this term leads to a steady state shift of the cantilever amplitude to a new point of equilibrium, and it changes the frequency and damping rate of the cantilever oscillations. Below we consider the time-dependent part of the amplitude x only. We take into account the phase fluctuations of the heterodyne laser field. (See Eq. (7).) We assume that the single mode heterodyne laser has a Lorentzian form of spectrum (7). To obtain an analytic solution, we use the Fourier transform equations corresponding to Eqs. (2,4). The Fourier transform of the interference term (the second term in the right side of Eq. (4)) gives the convolution of the Fourier amplitudes of the heterodyne and signal fields.

$$i\omega E_{h,s}(\omega) = -\frac{1}{2\tau_p}\left(E_{h,s}(\omega) - E^0_{h,s}(\omega)\right), \tag{5a}$$

$$\left(\omega_0^2 - \omega^2 - i\omega\Gamma\right)x(\omega) = A\int_{-\infty}^{+\infty} d\omega_1\left[E_h(\omega_1)E_s^*(\omega+\omega_0+\omega_1) + E_h^*(\omega_1)E_s(\omega_1+\omega_0-\omega)\right] + F(\omega)/m, \tag{5b}$$

where the following Fourier transformations were used

$$E_{h,s}(\omega) = \int E(t)e^{-i\omega t}dt,\ x(\omega) = \int x(t)e^{-i\omega t}dt.$$

We assume that the signal is the stationary broadband field emitted by a thermal object. The δ-correlated signal is given by the expression

$$\frac{cS}{8\pi}\left\langle E_s^{ext}(\omega)E_s^{ext*}(\omega')\right\rangle = P_s(\omega)\delta(\omega-\omega'), \tag{6}$$

where $P_s(\omega)$ is the spectral density of the signal power incident on the resonator. The heterodyne field is described as a stationary field with a Lorentzian spectral distribution. Although for many types of lasers the spectrum has a non-Lorentzian form, our assumption does not limit the generality of our conclusions because we assume below that the laser line width is much less than the line width of the signal

$$\frac{cS}{8\pi}\left\langle E_h^{ext}(\omega)E_h^{ext*}(\omega')\right\rangle = P_h\frac{\Gamma_h}{c\pi(\omega^2+\Gamma_h^2)}\delta(\omega-\omega'), \tag{7}$$

where P_h is the external heterodyne power. For the spectral components of the thermal noise force, we have

$$\left\langle F(\omega)F^*(\omega')\right\rangle = \delta(\omega-\omega')\frac{k_BTK\Gamma}{\omega_0^2\pi}. \tag{8}$$

In (8) $K=m\omega_0^2$ is the spring constant of a microcantilever, k_B is the Boltzmann constant; and T is the temperature. Below we calculate the minimal measurable spectral irradiance (MMSI) using the equality,

$$\left\langle x_s^2(t)\right\rangle = \left\langle x_T^2(t)\right\rangle, \tag{9}$$

where $\left\langle x_s^2(t)\right\rangle$ is the mean square amplitude of oscillations induced by the radiation pressure force neglecting thermal noise; and $\left\langle x_T^2(t)\right\rangle = k_BT/K$ is the thermal noise mean square amplitude. Note that the system of equations for a harmonic oscillator and the field in an optical cavity (Eqs. 5a,b) is nonlinear due to the nonlinear dependence of the field amplitude in the resonator on the microcantilever coordinate given by Eq. (3). We consider a linear approximation for the solution of Eqs. (5a,b). We assume that for realistic values of parameters the oscillation amplitude of the cantilever is much smaller than the region of dispersion of the optical resonator. Our numerical simulations, presented below, confirm this assumption. In this paper we are not interested in the nonlinear regime of the cantilever vibrations (when the amplitude of the cantilever vibrations is larger than the length of dispersion of the optical resonator). The equilibrium position of the microcantilever can be chosen to provide the maximal field enhancement inside the resonator. In this case Eq. (3) gives

$$E_{h,s}^0(\omega) = \frac{E_{h,s}^{ext}(\omega)T_0}{1-\mathrm{R}}. \tag{10}$$

We assume that the line width of the heterodyne source, Γ_h, the microcantilever resonance frequency, ω_0, and the damping rate, Γ, are much less than the bandwidth of the optical resonator, τ_p^{-1}: $\Gamma_h,\omega_0,\Gamma \ll \tau_p^{-1}$. The frequency deviation of the signal spectral components from the heterodyne carrier frequency is of the order of ω_0. (See Eq. (12) below.) These frequency differences are negligibly small compared with the resonator line width. Thus Eq. (10) could be satisfied simultaneously for the heterodyne field and for the signal field.

To calculate the mean square amplitude $\left\langle x_s^2(t)\right\rangle$, we use the solution of Eqs. (5a,b)

$$x_s(t) = A\int_{-\infty}^{\infty}d\omega_1\int_{-\infty}^{\infty}d\omega\frac{\exp(-i\omega_1 t)(E_h(\omega)E_s^*(\omega+\omega_0+\omega_1)+E_h^*(\omega)E_s(\omega+\omega_0-\omega_1))}{\omega_0^2-\omega_1^2-i\omega_1\Gamma}. \tag{11}$$

To calculate the square average of amplitude $\left\langle x_s^2(t)\right\rangle$, we have to take into account that the spectral components of the fields $E_{h,s}(\omega)$ are □correlated. Performing two integrations with □functions, and taking into account Eqs. (7,8,10,11), we obtain the following expression for the mean square amplitude:

$$\left\langle x_s^2(t)\right\rangle = B\int_{-\infty}^{\infty} d\omega_1 \int_{-\infty}^{\infty} d\omega \frac{P_s(\omega+\omega_0-\omega_1)}{(\omega^2+\Gamma_h^2)(\omega^2+\tau_p^{-2})[(\omega+\omega_0-\omega_1)^2+\tau_p^{-2}][(\omega_1^2-\omega_0^2)^2+\omega_1^2\Gamma^2]}, \tag{12}$$

where $B=\dfrac{T_0^4 P_h \Gamma_h}{4\pi m^2 c^2 (1-R)^4 \tau_p^4}$. The integrals in Eq. (12) are calculated assuming that (i) $\Gamma_h \ll \tau_p^{-1}$ and (ii) the signal spectral band is much broader than the line widths of the heterodyne laser and the optical resonator. Consequently, when calculating the integral over ω_1 in Eq. (12), we can take into account only the residuals of the denominator. Performing these straightforward calculations, we obtain

$$\left\langle x_s^2(t)\right\rangle = \frac{4\pi P_h \omega_0^2 T_0^4 [P_s(0)+P_s(2\omega_0)]}{c^2 K^2 \Gamma (1-R)^4}. \tag{13}$$

According to Eq. (12) the microcantilever senses the sum of two spectral components corresponding to the frequencies $\omega_s=\omega_h-\omega_0$ and $\omega_s=\omega_h+\omega_0$. As assumed above, the signal bandwidth is much larger than the cantilever frequency, ω_0. In our later considerations we will assume $P_s(0)=P_s(2\omega_0)$. Combining Eqs. (9) and (13) we obtain for the MMSI

$$I_{\min}=\frac{k_B T \rho d c^2 \Gamma (1-R)^4}{8\pi P_h T_0^4}, \tag{14}$$

where ρ is the density of the cantilever material, d is the thickness of the cantilever. We estimate the MMSI for values of parameters typical for two types of cantilevers. First is the thin and soft cantilever usually used for atomic force microscopy. Second is the micro-mirror with a very high coefficient of reflection utilized in the laser cooling experiments[10,11].

Example 1. In the case of a thin and soft cantilever, the typical values of parameters are: $\rho=2.33\times10^3 kg/m^3$, $d=60\ nm$, $\Gamma=2\pi\times10^2\ s^{-1}$, $\Gamma_h=2\pi\times10^8\ s^{-1}$, and $\lambda=10\ \mu m$, $T=300\ K$, $R=0.95$, $T_0^2=0.1$, and $P_h=10^{-3}\ W$. For these values of the parameters, Eq. (14) gives $MMSI=5.1\times10^{-6}\ W/m^2Hz$. The response time is $\tau=2\pi\ \Gamma^{-1}=10\ ms$. For chosen reflection coefficient, R, and the length of the resonator, $L=15\ \mu m$, the damping rate is, $2\tau_p^{-1}=5\times10^{11}\ s^{-1}$. Consequently, our assumption that $2\tau_p^{-1}\gg\Gamma_h,\ \omega_0,\ \Gamma$, is fulfilled. The dispersion length of the optical resonator is $l=(1-R)\lambda/(4\pi\sqrt{R})=40\ nm$. The average amplitude of the thermal oscillations is $\sqrt{\left\langle x_T^2\right\rangle}=\sqrt{k_BT/K}=0.65\ nm$. Thus, the condition of the validity of the linear approximation, $l\gg\sqrt{\left\langle x_T^2\right\rangle}$, is also fulfilled.

Example 2. In the second example we use the parameters of the micromirror obtained in recent laser cooling experiments[11]. In this case a mirror with an area $S=520\times120\ \mu m^2$, the parameters are: $S=520\times120\ \mu m^2$, $\omega_0=278.3$ KHz, $\rho=2.67\times10^3\ kg/m^3$, $d=2.4\ \mu m$, $\Gamma=2\pi\times13\ s^{-1}$, and $T=300\ K$, $R=0.998$, $T_0^2=1-R=2\times10^{-3}$,

$P_h = 10^{-1}\ W$. In this case, $MMSI = 1.95\times10^{-9}\ W/m^2Hz$. The response time is $\tau = 2\pi\ \Gamma^{-1} = 77\ ms$. Comparison of these two cases shows that the most critical parameter is the coefficient of reflection, R. The value of the reflectance obtained for micromechanical Bragg mirrors[10,11] is not highest for this technology. As the authors[11] note, the Bragg mirror technology can provide reflection coefficients even higher than 0.999999. Micromirrors with reflectance 0.9999 for infrared radiation are commercially available. A micromirror with reflectance 0.9999 was demonstrated recently in laser cooling experiments[12]. The highest micromirror reflection coefficient, 0.999985, was demonstrated in ring down microscopy[13]. The adaptation of this technology leads to a tremendous improvement in the sensitivity. For example, using the value of a reflection coefficient $R = 0.9999$, and the values of others parameters used in Example 2, we obtain $MMSI = 4.87\times10^{-12}\ W/(m^2Hz)$. The microcavity with flat mirrors such as used in[9] has diffraction losses (leak losses) which can exceed the transmission losses in the case of a very high reflectivity. The efficient solution of this problem was realized in[14], where the mirror of Fabre-Perot microresonator consists of the movable and unmovable parts. Because of the oscillation amplitude of the movable part of the mirror is negligible small, it does not affect the resonator losses. At the same time, the total area of the mirror is large enough to avoid the diffraction losses. In our estimates in Example 2 we assume that micromirror consists of the movable and unmovable parts, and the size of movable part, $S = 520\times120\ \mu m^2$, is significantly smaller than the size of unmovable part. According to the expression (14), the MMSI is proportional to thickness of the mirror. To obtain higher sensitivity we need the thinner mirror. However, the mirror technology limits the thickness depending on size of the mirror. Thus, the smaller area of a movable mirror the smaller thickness can be manufactured. For example, using the movable mirror size of the order of the wavelength, $10\times10\ \mu m^2$, we can assume that the thickness is of the order of 240 nm, instead 2.4 μm which we use in the Example 2. In this case, the MMSI estimate above becomes less by an order of magnitude. Note that microcavity with curved mirrors in stable paraxial geometry, such as used in[10], also overcomes the problem of diffraction losses. For comparison of the sensitivity of the proposed spectrometer with a standard IR-spectrometer with uncooled detector, consider a numerical example. We assume that conventional IR spectrometer is equipped with a photosensor array, in which an individual pixel is a microbolometer. We assume also that the conventional spectrometer operates in the spectral interval, 8- 14 μm, and has the same spectral resolution as the proposed spectrometer. In our case, the spectral resolution is defined by the laser line width, which we choose equal to $\Delta\nu = 30$ MHz. For a conventional spectrometer, this high spectral resolution can be achieved in combination with a Fabry-Perot etalon. The theoretical limit for NETD of a microbolometer with pixel size of $30\times30\ \mu m^2$ is 5 mK (experimental sensitivity is 20-50 mK). Our estimate uses NETD = 20 mK. The minimal measurable spectral irradiance is $MMSI = NETD\times(dP/dT)_{\lambda_1-\lambda_2}\times(\Delta\nu)^{-1}$, where $(dP/dT)_{\lambda_1-\lambda_2}$ is the slope of the black body radiation within the spectral band 8-14 μm: $(dP/dT)_{\lambda_1-\lambda_2} = 2.62\ Wm^{-2}K^{-1}$. For $\Delta\nu = 30$ MHz, NETD = 20 mK we get $MMSI = 1.75\times10^{-9}\ \mathrm{W/(m^2\ Hz)}$. Thus, the microcantilever spectrometer has a sensitivity that is almost three orders of magnitude better.

THz-spectrometer: Comparison with existing technology

In our estimates we use the specifications of a commercially available terahertz source, based on a CO_2 gas cell pumped by a sealed CO_2 laser (Coherent Inc.), which provides P_h = 100 mW with a line width of $\Delta\nu = 50$ KHz, and has frequency-tuning interval of 0.3 THz - 4 THz. The highest reflection coefficient, 0.997, for this spectral region was observed for thin metal film on glass substrate[15]. The MEOMS mirror area is $S = 300\times300\ \mu m^2$. The minimal spectral irradiance is $P_{min} = 4.4\times10^{-10}W/(m^2Hz)$. The noise equivalent power for a conventional THz uncooled bolometer is $NEP = 10^{-12}$ W/Hz$^{1/2}$ at the measurements bandwidth, $\delta\nu = 30$ Hz. The minimal measurable value of the spectral density is $P_{conv} = NEP\times(\delta\nu)^{1/2}\times(\Delta\nu)^{-1}\times S^{-1} = 1.2\times10^{-9}$ W/(m^{2}Hz). Thus theoretical sensitivity of the proposed THz spectrometer is comparable with conventional spectrometers. In our estimates we use a rather high quality factor for the

microcantilever oscillator, $\omega_0/\Gamma = 10^3 - 2\times10^4$. This quality factor is typical for microcantilevers placed in a vacuum chamber. The vacuum technology is well developed and is commonly used in microcantilever based thermal imagers[4].

III. THE NOISE CONTRIBUTION FROM LASER INTENSITY FLUCTUATIONS

In our sensitivity analysis in Section II, we take into account explicitly the phase noise in the form of the spectral distribution of the field correlation moment in Exp. (7). However, the intensity fluctuation of the heterodyne laser gives an additional contribution to the system noise due to the first term in the right side of Eq. (4). To take into account this part of the noise, we present the heterodyne laser power in the form $P^{\text{int}}{}_h(t) = \overline{P}_h^{\text{int}} + \delta P_h(t)$, where the term $\delta P_h(t)$ is the intensity fluctuations. To calculate the contribution of the intensity fluctuations to the amplitude oscillations $x(t)$, we consider Eq. (4) without the second and third terms on the right side of the equation

$$\ddot{x} + \Gamma\dot{x} + \omega_0^2 x = 2\delta P/cm. \tag{15}$$

Using Eq. (15) we can write the equation for the spectral amplitude

$$(\omega_0^2 - \omega^2 - i\Gamma\omega)x(\omega) = \frac{2\delta P_h(\omega)}{cm}, \tag{16}$$

where the correlation moment of $\delta P_h(\omega)$ is given by

$$\left\langle \delta P(\omega)\delta P(\omega')\right\rangle = \delta(\omega+\omega')\left(\overline{P}_h^{\text{int}}\right)^2 RIN(\omega), \tag{17}$$

where $RIN(\omega) = \dfrac{\left\langle \delta \mathrm{P}^2(\omega)\right\rangle}{\left(\overline{\mathrm{P}}_{\mathrm{h}}^{\text{int}}\right)^2}$ is the relative intensity noise. The average square oscillation amplitude is given by

$$\left\langle x_N^2(t)\right\rangle = \iint d\omega d\omega' \exp[i(\omega+\omega')t]\left\langle x(\omega)x(\omega')\right\rangle. \tag{18}$$

Using the solution of Eq. (16) we obtain

$$\left\langle x_N^2(t)\right\rangle = \frac{4\pi\overline{P}_h^2 RIN(\omega)}{c^2m^2\omega^2\Gamma(1-R)^2}, \tag{19}$$

where $\overline{P}_h^{\text{int}} = \overline{P}_h/(1-R)^2$. Let's estimate $RIN(\omega)$ for the case in which fluctuations of oscillation amplitude of the micromirror $x_N(t)$ due to the laser intensity noise are comparable with thermal fluctuations. From equality $\left\langle x_N^2(t)\right\rangle \simeq \dfrac{k_bT}{m\omega^2}$ we get

$$RIN(\omega) = \frac{k_bTc^2m(1-R)^2\Gamma}{2\overline{P}_h^2}. \tag{20}$$

For values of parameters: $m = \rho\times S\times d$, S=520×120 μm^2, ρ=2.67×10^3 kg, d=2.4 μm, R=0.9999, Γ=30 Hz, $\overline{\mathrm{P}}_{\mathrm{h}} = 0.1$ W we get $RIN(\omega) = -16.85$ dB/Hz. The considerations above show that to obtain the thermal fluctuation limit, one must use a laser with a rather low relative intensity noise, $RIN \leq$ -17 dB/Hz.

In recent experiments it was shown that a quantum cascade (QC) laser has this value of RIN at a temperature of 88 K, and for the laser power of about of several tens of mW[16]. Theoretical analysis shows that this value of RIN can be obtained at room temperature as well[17].

IV. THERMAL RADIATION DETECTOR

Thermal imaging usually exploits broad band infrared radiation corresponding to the window of atmospheric transparency 8 – 14 μm. For these applications we consider a scheme in which the IR radiation intensity is modulated by the optical modulator at a frequency equal to the resonance cantilever frequency, ω_0. To fulfill the resonance condition for each spectral component of the thermal radiation broad spectrum, it is necessary to send different spectral components at certain different angles. The resonance condition in the microcavity is $L\cos\theta = \frac{\lambda}{2}N$, where L is the initial length of the microcavity, θ is the angle between the microcavity axis and the direction of propagation of the light (see Fig. 2), $N = 1,2,3....$ The different wavelengths correspond to the different angles, at which the resonance condition is fulfilled. It is possible to obtain these conditions using a diffraction micrograting with a surface oriented perpendicular to the surface of the micricavaties. (See Fig. 2). The diffraction angle satisfies the condition, $l\cos\theta = \lambda$, where l is the period of the grating. We assume to utilize microgratings with a single diffraction maximum. Both resonance conditions lead to a relationship between the microcavity length and the grating period, $l = 2LN^{-1}$. All microoptical elements could be fabricated as a monolithic matrix and bonded with the microcavity matrix.

The motion of the micromirror is described as the motion of a harmonic oscillator perturbed by a time modulated radiation pressure force and by thermal noise:

$$\ddot{x} + \Gamma\dot{x} + \omega_0^2 x = AM(t)\left|E_s\right|^2 + \frac{F}{m}, \tag{21}$$

where $M(t)$ is the power modulation function, $M(t) = 0.5[1 + r\cos(\omega_0 t)]$, F is the thermal noise force. As in section 2, we assume that the resonance frequency ω_0 and the damping rate Γ are much less than bandwidth of the microcavity. We assume also that the amplitude oscillation of mirror is much smaller than the wave length. Thus, the intensity inside and outside the microcavity are related through the formula for stationary fields:

$$I_s = \frac{I_s^{ext} T_0^2}{(1-R)^2}. \tag{22}$$

The solution of Eq. (21) can be written in the form $x(t) = x_0 + \frac{1}{2}x_s \exp(i\omega_0 t) + c.c.$, where x_0 is a constant shift of the micromirror from its equilibrium position. The expression for x_s can be found from Eq. (21)

$$x_s^2 = \frac{(I_s^{ext} S)^2}{2m^2\omega_0^2 c^2 \Gamma^2 (1-R)^2}. \tag{23}$$

In the expression (23) we assumed that $T_0^2 = 1 - R$.

The average square amplitude of the micromirror oscillations induced by the thermal noise is:

$$\left\langle x_T^2(t)\right\rangle = \frac{k_B T}{m\omega_0^2}. \tag{24}$$

The minimal measurable value of intensity is given by the equality:

$$\left\langle x_s^2(t)\right\rangle = \left\langle x_T^2(t)\right\rangle. \tag{25}$$

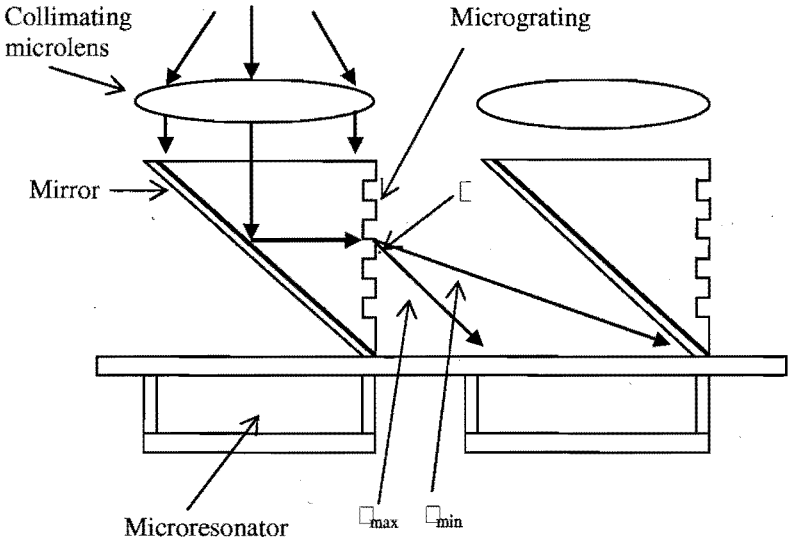

Fig. 2. Setup of the broadband thermal radiation detector.

From equality (25) we get

$$I_{s\min}^{ext} = \left[\frac{2\rho dc^2\Gamma^2 k_B T(1-R)^2}{S}\right]^{1/2}. \tag{26}$$

The noise equivalent temperature difference (NETD) is:

$$NETD = I_{s\min}^{ext}[(dP/dT)_{\lambda_1-\lambda_2}]^{-1}, \tag{27}$$

where ρ is the density of the micromirror material and d is the micromirror thickness. We choose the following values of microcavity parameters: $S = 140\times140\ \mu\text{m}^2$, $\rho = 2.33\times10^3\ \text{kg/m}^3$, $(dP/dT)_{\lambda_1-\lambda_2} = 2.62\ \text{Wm}^{-2}K^{-1}$, $d = 1\ \mu\text{m}$, $\Gamma = 30\ \text{Hz}$, $T = 300\ ^\circ K$, $R = 0.99999$, $\omega_0 = 4.5\ \text{MHz}$. For these values of the parameters Eq. (27) gives, $\text{NETD} = 6.8\ \text{mK}$. Additional progress in the reflection coating potentially leads to significantly higher sensitivity. Thus, for the reflection coefficient, $\text{R} = 0.999999$ and for the same values of other parameters as used above, we have $\text{NETD} = 0.68\ \text{mK}$. To compare the sensitivity our opto-mechanical detector with the sensitivity of conventional microbolometers, one must take into account that the sensitivity of the conventional microbolometer is inversely proportional to the photosensitive area. If the sensitivity of conventional microbolometer with the area, $50\times50\ \mu\text{m}^2$, is 10 mK (Raytheon[18]), then for a microbolometer with the area, $140\times140\ \mu\text{m}^2$, the sensitivity is 1.275 mK. Thus our opto-

mechanical detector potentially has a sensitivity comparable with the best conventional microbolometer. Although the theoretical limit for the conventional microbolometer is lower, this limit cannot be achieved without severe performance compromises. Practical devices typically lag theoretical performance by a factor of 3 to 6. These limitations are due to the physics of the detection strategy and are not shared by a radiation pressure sensor. By measuring changes in resistance, capacitance or banding of a microcantilever, conventional bolometers actually measure temperature changes ΔT due to radiation absorption. The dynamic thermal exchange between the detector and its surroundings is one of the fundamental noise sources that appear as fluctuations in the detector temperature. The sensitivity of these measurements is limited by temperature fluctuations δT, which leads to square root dependence of NETD on thermal conductance $\mathrm{NETD_{TF}} \sim \sqrt{\mathrm{G_T}}$, where $\mathrm{NETD_{TF}}$ is that part of NETD due to temperature fluctuations. For example, a bolometer based on a bimaterial microcantilever array has the theoretical limit for temperature fluctuation noise, NETD=6.56 mK[3]. To reduce this limit, high thermal isolation is needed. However, the highest thermal isolation is limited by the requirement for fast response time of the imager, which is inversely proportional to the thermal conductance G_T^{-1}. In the radiation pressure sensor, the sensitivity limit is determined by the thermo-mechanical noise, which depends on the square root of the average temperature T, but not on fluctuations. (See Eq. (26).) As a result, our method is practically insensitive to temperature fluctuations. This is one of the main advantages of our approach.

V. NUMERICAL SIMULATIONS

For numerical simulations we use Eqs. (2,4). The thermal noise and the signal are simulated by a standard random number generator, which produces a random sequence of pulses. The time duration of these pulses, Δt, is much shorter than the oscillation period of the microcantilever, $T = 2\pi/\omega_0 = 40\Delta t$. The probability of the pulse amplitude is uniform in the interval $\left[-a_{th,s}, a_{th,s}\right]$. To avoid undesirable correlations between the signal and thermal noise processes, we use two different random pulse generators. We find that for nonlinear oscillations, when the amplitude of thermal oscillations, x_T, is comparable with the optical resonator dispersion length, l, the nonlinearity leads to a significant decrease in the signal-to-noise ratio. Thus, the nonlinearity is an undesirable feature. The values of parameters, chosen above in Section II, provide a linear regime of microcantilever oscillations. To control the linearity, we calculate the mean square amplitude only for the thermal noise $\left\langle x_T^2(t)\right\rangle$ of the cantilever (without a signal). Then, we calculate the mean square signal amplitude $\left\langle x_s^2(t)\right\rangle$ which includes the thermal noise of radiation but does not include the thermal noise of the cantilever. Finally, we calculate the mean square amplitude $\left\langle x^2(t)\right\rangle$ for conditions in which both noises, of the radiation and of the cantilever exist. In the linear case, the last sum is equal to the sum of the mean square amplitudes calculated separately:

$$\left\langle x^2(t)\right\rangle = \left\langle x_T^2(t)\right\rangle + \left\langle x_s^2(t)\right\rangle .$$

As shown in Section II, the highest sensitivity is obtained when the optical resonator is tuned to exact resonance with the both heterodyne and the signal fields. However, the non-resonant term in Eq. (4) induces a shift of the equilibrium position of the amplitude of oscillations. Nevertheless, the optimal position can be obtained by introducing an initial off-set of the position of the cantilever relative to the resonance. This could be achieved, for example, by using a feedback loop which measures the level of the heterodyne intensity after passing the resonator and feeds it back to a piezo-ceramic substrate which shifts the initial position of the cantilever. The dependence of the optimal equilibrium position of the cantilever, x_e, on the heterodyne power for different initial deviation, x_0, is presented in Fig. 3. These dependences demonstrate the well-known[19] bi-stable type of curves. To avoid undesirable instability, a practically acceptable region must be chosen outside of the bi-stable region. The dependence of the MMSI on the heterodyne external power, P_h, for the optimal initial deviation

for each value, P_h, is presented in Fig. 4. As can seen, the value $P_h = 10^{-3}\ W$ corresponds to $MMSI = 3.5\times10^{-6}\ W/m^2Hz$, which is in qualitative agreement with the analytical estimate given in Section 2 (Example 1) for the same value of the heterodyne power, $MMSI = 5.1\times10^{-6}\ W/m^2Hz$.

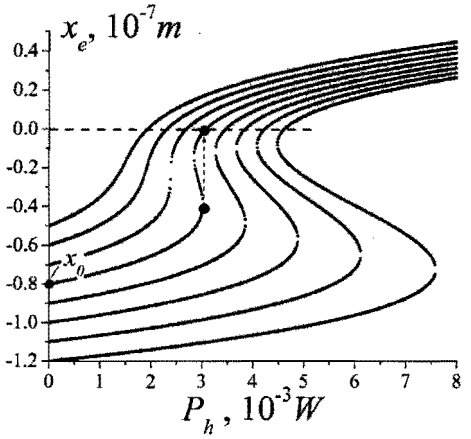

Fig. 3. Dependence of a microcantilever equilibrium position x_e on the power of the heterodyne laser.

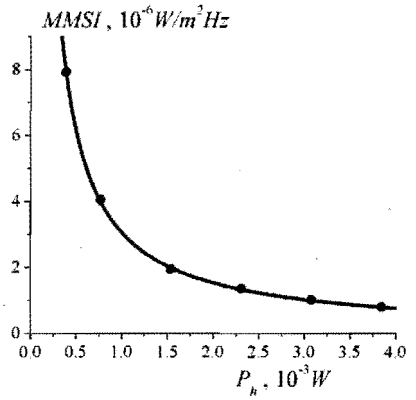

Fig. 4. Dependence of MMSI on the heterodyne power.

The dependence of the MMSI on the heterodyne external power, P_h, for the optimal initial deviation for each value, P_h, is presented in Fig. 4. As can seen, the value $P_h = 10^{-3}\ W$ corresponds to $MMSI = 3.5\times10^{-6}\ W/m^2Hz$, which is in qualitative agreement with the analytical estimate given in Section 2 (Example 1) for the same value of the heterodyne power, $MMSI = 5.1\times10^{-6}\ W/m^2Hz$.

VI. CONCLUSION

We have described a far infrared (terahertz), uncooled detector based on a micromirror as a radiation pressure sensor for spectroscopic applications and for imaging. This radiation pressure sensor potentially has sensitivity at the level and better than the best conventional uncooled detectors.

VII. AKNOWLEGMENT

This work was carried out under the auspices of the National Nuclear Security Administration of the U.S. Department of Energy at Los Alamos National Laboratory under Contract No. DE-AC52-06NA25396.

REFRENCES

[1]. Manalis, S.R, Minne, S.C., Quate, C.F., Yaralioglu, G.G., and Atalar, A., "Two-dimensional micromechanical bimorth arrays for detection of thermal radiation", Appl. A., Phys. Lett. 70, 3311 (1997).
[2] Perazzo, T., Mao, M., Kwon, O., Majumdar, A., Varesi, J.B.,and Norton, P., "Infrared vision using uncooled micro-optomechanical camera", Appl. Phys. Lett. 74, 3567 (1999).
[3] Datskos, P.G., Lavrik, N.V., and Rajic, S., "Performance of uncooled microcantilever thermal detectors", Rev. Sci. Instrum. **75**, 1134 (2004).
[4] Li, C.B., Jiao, B.B., Shi, S.L., Chen, D.P., Ye, T.C., Zhang, Q.C., Guo, Z.Y., Dong, F.L., and Miao, Z.Y., "A novel uncooled substrate-free optical-readable infrared detector: design, fabrication and performance", Meas. Sci. Technol. 17, 1981(2006).
[5] Chernobrod, B.M., Berman, G.P., and Milonni, P.W., "Improving the sensitivity of frequency modulation spectroscopy using nanomechanical cantilever", Appl. Phys. Lett. 85, 3896 (2004).
[6] Berman, G.P., Bishop, A.R., Chernobrod, B.M., Hawley, M.E., and Brown, G.W. "Sensitivity analysis of a proposed novel opto-nano-mechanical photodetector for improving the performance of LIDAR and local optical sensors", J. Phys.: Conference Series 38, 171 (2006).
[7] http://www.cascade-technologies.com/docs/LaserSystemLS01.pdf
[8] http://www.laser2000.de/index.php?id=366435&L=1
[9] Metzger, C.H. and Karrai, K., "Cavity cooling of a microcantilever", Nature 432, 1002 (2004).
[10] Gigan, S., H.R. Böhm, M. Paternostro, F. Blaser, G. Langer, J.B. Hertzberg, Schwab, K.C., Bäuerle, D., Aspelmeyer, M., and Zeilinger, A.,"Self-cooling of a micromirror by radiation pressure", Nature 444, 67 (2006).
[11] Böhm, H.R., Gigan, S., Blaser, F. , Zeilinger, A., Aspelmeyer, M., Langer, G., Bäuerle, D., Hertzberg, J.B., and Schwab, K.C., "High reflectivity high-Q micromechnical Bragg mirror", Appl. Phys. Lett. 89, 223101 (2006).
[12] Arcizet, O., Cohadon, P.-F., Briant, T., Pinard, M., and Heidmann, A., "Radiation pressure cooling and optomechanical instability of a micromirror ", Nature 444, 71 (2006).
[13] Mabuchi, H., Turchette, Q.A., Champman, M.S., and Kimble, H.J., "Real-time detection of individual atoms falling through a high-finesse optical cavity", Opt. Lett. 21, 1393 (1996).
[14] Favero, I., Metzger, C., Camerer, S., König, D., Lorenz, H., Kotthaus, J.P., and Karrai, K., „Optical cooling of a micromirror of wavelength size", Appl. Phys. Lett., 90, 104101 (2007).
[15] Gatesman, A.J., Giles, R.H., and Waldman, J., "High-precision reflectometer for submillimeter wavelengths", JOSA B 12, 212 (1995).
[16] Gensty, T., Elsäßer, W., and Mann, C., "Intensity noise properties of quantum cascade laser", Opt. Express 13, 2032 (2005).
[17] Gensty T. and Elsäßer, W., "Semiclassical model for the relative intensity noise of intersband quantum cascade lasers", Opt. Commun. 256, 171 (2005).
[18]] Murphy, D., Ray, M., Wyles, J., Asbrock, J., Hewitt, C., Wyles, R.,. Gordon, E., Sessler T., Kennedy, A., Baur, S., Van Lue, D., Anderson, S., Chin, R., Gonzales, H., Le Pere, C., Ton, S., and Kostrzewa, T., "Performance improvement for VOx microbolometer FPAs", Infrared Technology and Application XXX, edited by B. F. Andresen, G. F. Fulop, Proc. of SPIE, 5406, 531 (2004).
[19] Dorsel, A., McCullen, J.D., Meystre, P., Vignes, E., and Walther, H., "Optical bistability and mirror confinement induced by radiation pressure", Phys. Rev. Lett. 5,1550 (1983).